JOURNAL OF GEOPHYSICAL RESEARCH, VOL. 113, B05411, doi:10.1029/2007JB005228, 2008

Spontaneous generation of pure ice streams via flow instability: Role of longitudinal shear stresses and subglacial till

Roiy Sayag[1] and Eli Tziperman[1]

Received 13 June 2007; revised 26 December 2007; accepted 1 February 2008; published 30 May 2008.

[1] A significant portion of the ice discharge in ice sheets is drained through ice streams, with subglacial sediment (till) acting as a lubricant. The known importance of horizontal friction in shear margins to ice stream dynamics suggests a critical role of longitudinal stresses. The effects of subglacial till and longitudinal stresses on the stability of an ice sheet flow are studied by linear stability analysis of an idealized ice-till model in two horizontal dimensions. A power law-viscous constitutive relation is used, explicitly including longitudinal shear stresses. The till, which has compressible viscous rheology, affects the ice flow through bottom friction. We examine the possibility that pure ice streams develop via a spontaneous instability of ice flow. We demonstrate that this model can be made intrinsically unstable for a seemingly relevant range of parameters and that the wavelengths and growth rates that correspond to the most unstable modes are in rough agreement with observed pure ice streams. Instabilities occur owing to basal friction and meltwater production at the ice-till interface. The most unstable wavelength arise because of selective dissipation of both short and long perturbation scales. Longitudinal stress gradients stabilize short transverse wavelengths, while Nye diffusion stabilizes long transverse wavelengths. The selection of an intermediate unstable wavelength occurs, however, only for certain parameter and perturbation structure choices. These results do not change qualitatively for a Newtonian ice flow law, indicating no significant role to shear thinning, although this may very well be due to the restrictive assumptions of the model and analysis.

Citation: Sayag, R., and E. Tziperman (2008), Spontaneous generation of pure ice streams via flow instability: Role of longitudinal shear stresses and subglacial till, *J. Geophys. Res.*, *113*, B05411, doi:10.1029/2007JB005228.

1. Introduction

[2] Ice streams (IS) in Antarctica provide a drainage system that covers merely 10% of the surface, yet accounts for about 90% of the ice sheet discharge [*Bamber et al.*, 2000]. Pure IS (as opposed to topographic ones), such as those at the Siple coast at the west Antarctica ice sheet, are typically 50 km wide and 300–500 km long. Their average thickness is 1 km and the flow velocity is 100–800 m a^{-1}, 2–3 orders of magnitude faster than the meters per year velocity of the surrounding ice sheet [*Whillans et al.*, 2001]. The surface slopes of pure IS are 10^{-3}–10^{-4} and they can flow over a layer of subglacial porous sediment (till), which is meters thick and can dilate due to meltwater and hence facilitate sliding. These ice streams vary in time, at times crossing the path of older inactive streams [*Jacobel et al.*, 1996], and it seems, therefore, that the location of these ice streams is not dictated by the topography and that these streams can develop over a homogeneous base [*Bentley*, 1987]. In spite of their importance in both present and past ice sheet dynamics, it is probably fair to state that a fundamental understanding of the formation mechanism of pure IS and the associated spatial scales is still incomplete.

[3] *Kamb* [2001] observed that subglacial deformation accounts for 80–90% of the motion in Bindschadler ice stream but only for 25% of that of Whillans ice stream (both IS at Siple coast). He also observed that the hydraulic systems of the active and inactive Siple coast IS are very similar. This implies that the formation and existence of pure IS depends on additional controls to the basal meltwater presence and consequential sliding. The gravitational driving forces due to the downslope weight of ice streams may be largely balanced by friction due to longitudinal stresses in the side shear zones of the ice streams, with the rest balanced by bottom friction [*Raymond et al.*, 2001; *Jackson and Kamb*, 1997]. These 4–5 km wide shear zones are visible at the IS margins, where intense deformation gives rise to surface crevasses and fractures [*Echelmeyer et al.*, 1994]. The driving stresses of the Siple coast IS are mostly substantially under 100 kPa along their flow line [*Bindschadler et al.*, 2001]. The IS shear zones, in comparison, can support shear stresses greater than 100 kPa, an

[1]Department of Earth and Planetary Science and School of Engineering and Applied Sciences, Harvard University, Cambridge, Massachusetts, USA.

0148-0227/08/2007JB005228$09.00

order of magnitude more than the capability of basal stresses in some cases.

[4] The purpose of this work is to study the possibility that pure ice streams develop as a spontaneous instability of ice sheet flow over a homogeneous base. More specifically, we are interested in the role of longitudinal stresses in combination with bottom processes in the development of pure ice streams. Our approach is to use linearized stability analysis of a uniform horizontal shear flow of a vertically averaged ice flow model, overlying a layer of subglacial sediment, in two horizontal dimensions.

[5] Previous studies approached some aspects of ice stream formation using different methods. *Fowler and Johnson* [1996, 1995] demonstrated a hydraulic run-away mechanism of thermomechanically coupled flow based on the positive feedback between sliding velocity and basal meltwater production. This mechanism is closely related to the instability studied in this paper. Given that ice stiffness can change by 3 or more orders of magnitude as function of the temperature [*Paterson*, 1994; *Marshall*, 2005] and that this can result in an instability based on the positive feedback between dissipation, temperature, and viscosity, quite a few studies considered the role of thermoviscous coupling in the formation and dynamics of ice streams [*Fowler and Larson*, 1980; *Nye and Robin*, 1971; *Clarke et al.*, 1977; *Yuen and Schubert*, 1979]. However, these studies typically ignored the cross-stream horizontal dimension and therefore cannot predict critical dynamical factors such as the width of ice streams. *Schoof* [2006] developed a variational approach to determine the spatial extent and flow velocities of ice streamflow for a given ice sheet geometry and distribution of basal yield stresses. Other numerical studies included the cross stream horizontal dimension [e.g., *Pattyn*, 2003, 1996; *Payne and Dongelmans*, 1997; *Saito et al.*, 2006; *Marshall and Clarke*, 1997; *Hubbard et al.*, 1998; *Ritz et al.*, 2001; *Macayeal*, 1992; *Huybrechts et al.*, 1996; *Hulton and Mineter*, 2000] and found interesting switching behavior of ice stream-like features. Many of these studies used the shallow ice approximation, which was called into question in this context by recent work [*Hindmarsh*, 2006b, 2004b; *Gudmundsson*, 2003], and in those that solved the full stokes problem, the model complexity makes it difficult to isolate the role of longitudinal stresses.

[6] *Hindmarsh* [2004a] performed a thorough linear stability analysis of a horizontally uniform mean flow, in a detailed three-dimensional thermoviscous coupled ice sheet model based on the shallow ice approximation (SIA), as function of horizontal wavelengths. *Hindmarsh* [2006b] then found that the use of the SIA can bias the instability analysis results. Maximum growth rates at a finite transverse (cross-stream) wavelength were observed in some cases, but the associated wavelengths were too long to explain observed IS spacing and width. He concluded that thermoviscous instabilities are unlikely to result in a spontaneous development of ice streams. *Hindmarsh* [2006b] also demonstrated using a simpler model based on *Macayeal* [1989] and Newtonian rheology ($n = 1$ in Glen's law [*Glen*, 1952]) that the introduction of longitudinal stresses damps instabilities. *Balmforth et al.* [2003] also demonstrated the stabilizing effects of longitudinal stresses.

[7] In contrast to the above, we are interested here in the potential destabilizing non-Newtonian effects of longitudinal stresses due to shear thinning effects. A small perturbation to the flow which increases the strain rate, will reduce the effective viscosity (shear thinning), and therefore result in a growth of the perturbation and a positive destabilizing feedback. Consider a rough estimate of this effect in the context of ice streams. The effective viscosity under Glen's law is $\mu = \frac{1}{2}B\dot{\epsilon}_{II}^{[(1/n)-1]}$, where the second invariant of the rate of strain tensor is $\dot{\epsilon}_{II}^2 = \frac{1}{2}\dot{\epsilon}_{ij}\dot{\epsilon}_{ij}$, and B is the temperature-dependent ice stiffness parameter. Assuming plug flow in the context of ice streams, the rate of strain is dominated by the horizontal shear within the shear margins which can be scaled as U_{IS}/L, with a typical ice stream velocity, $U_{\mathrm{IS}} = 1\ \mathrm{km\ a^{-1}}$, and the width of ice stream shear margins, $L = 5$ km. In the interior of the ice sheet, the dominant rate of strain is due to the vertical shear, and is of the order of U_{interior}/H, where we can use $U_{\mathrm{interior}} = 1\ \mathrm{m\ a^{-1}}$ and an ice sheet thickness scale of $H = 3$ km. We therefore have, for $n = 3$ and a constant B, an order of magnitude estimate,

$$\frac{\mu_{\mathrm{IS}}}{\mu_{\mathrm{interior}}} \approx \left(\frac{U_{\mathrm{IS}}/L}{U_{\mathrm{interior}}/H}\right)^{\left(\frac{1}{n}-1\right)} \approx 0.015. \tag{1}$$

The effective viscosity can therefore change by 2 orders of magnitude, which may result in interesting dynamics regardless of the potentially larger temperature induced changes in B. The shear thinning effect exists, of course, only for $n > 1$, which results in a significantly more complicated mathematical problem than the Newtonian case of $n = 1$. In order to be able to investigate these effects we therefore neglect many other physical factors that are known to be equally or even more important.

[8] Bottom sliding, of course, is a feedback that cannot be neglected even in the simplest analysis of ice stream formation. Laboratory studies show that till behaves like granular material and is probably best modeled with plastic rheology [*Tulaczyk et al.*, 2000a]; yet it is unclear how the resulting deformation should be modeled [*Fowler*, 2003]. In fact some observations seem better fit with viscous rheology [*Hindmarsh*, 1997, 1998]. A regularized coulomb friction law to model basal sliding with cavitation was suggested by *Schoof* [2005] and *Gagliardini et al.* [2007]. We assume the ice to flow over a compressible viscous till layer, resulting in a basal drag coefficient for the ice flow that varies with the net meltwater content, as motivated by *Tulaczyk et al.* [2000a] and *Tulaczyk et al.* [2000b]. Our till dynamics are far simpler than those used, for example, by *Dell'Isola and Hutter* [1998] and *Balmforth et al.* [2003] and is essentially meant to crudely represent the positive destabilizing feedback between basal friction and melt water production, and the enhanced flow speed [*Fowler and Johnson*, 1996, 1995].

[9] Our model geometry, like the physical processes included, is highly idealized. The ice sheet flow is confined within fixed side boundaries and perturbations to the mean flow are assumed periodic in the along-flow direction. This latter assumption is clearly not realistic as a description of ice streams in Antarctica or other ice sheet, yet it is commonly made when studying idealized instability models of fluid flow when one is interested in the cross-flow dynamics. Similarly, although our neglect of vertical shear cannot be justified away from the ice stream where it is

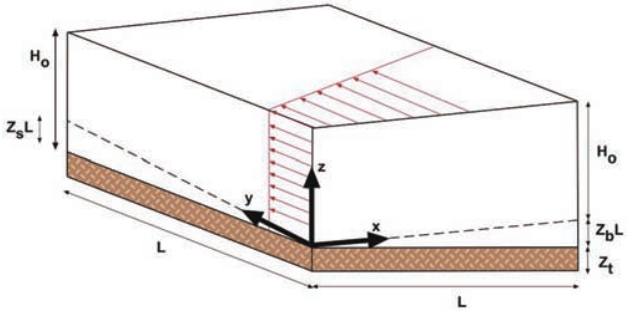

Figure 1. The geometry and components of the ice-till model. We use Cartesian coordinates (x, y) for the (across-mean flow, along mean flow) horizontal directions, and z for the upward direction, as shown. The ice surface is at z_s, and the bed is at z_b. The mean flow (thin arrows) has a shear in the direction perpendicular to the mean flow.

dominant, neglecting vertical shear within the ice stream and away from the bottom shear zone, may not be a bad assumption [*Fowler and Johnson*, 1996, 1995; *Macayeal*, 1989]. This assumption is also motivated here by our wish to allow physical insight via simplification of the model to include only the absolutely necessary elements that are needed to represent the two processes which are the focus of this study.

[10] The main novel elements introduced here are, first, the attempt to account for the shear thinning feedback (and hence the use of non Newtonian flow law with $n > 1$) in an analytic (or semianalytic) stability study; second, the combined investigation of bottom sliding due to meltwater production and longitudinal stresses, and, third, the analysis of the linear stability of a horizontally sheared flow as opposed to a horizontally uniform flow that was considered in previous studies [*Hindmarsh*, 2006b, 2004a]. The effective viscosity becomes singular if the equations are linearized about a mean flow with no shear, and linearizing around a shear flow as we do here is one of several possible ways of regularizing the flow law [*Baral et al.*, 2001; *Hutter*, 1983; *Jóhannesson*, 1992].

[11] We strongly emphasize that this is meant to be a concept paper, where we attempt to identify the role of only two specific processes that may be relevant to ice stream development, the shear thinning via longitudinal stresses and bottom friction/sliding feedback. In order to do so we neglect many other important factors such as the temperature dependence of the viscosity and therefore the entire set of thermoviscous couplings [*Hindmarsh*, 2004a] and vertical shear within the ice, we choose an idealized flow geometry, and we abandon realism to allow a better analysis and understanding of the dynamics.

[12] The existence of pure ice streams of a given width over homogeneous bottom that does not dictate a priori this width implies both an instability mechanism that results in the formation of these streams, and also stabilizing feedbacks at longer and shorter cross-stream wavelengths. By studying the simple ice flow model, we are able to point to potential stabilizing feedbacks at both short and long scales. Specifically, flow instability occurs due to the bottom sliding feedbacks rather than to the shear thinning feedback; basal friction results in meltwater production which weakens the till, leads to faster flow and to more basal heating and meltwater production, and therefore to a positive feedback which results in an instability similar to that of *Fowler and Johnson* [1996, 1995]. We also discuss potential extensions that may result in shear thinning playing a more dominant destabilizing role. Stability at short transverse (cross-stream) wavelengths is due to momentum dissipation by longitudinal shear stresses, as by *Hindmarsh* [2006b]. At long transverse wavelengths, stability occurs below a threshold along-flow wavelength due to Nye diffusion [*Nye*, 1959; *Gudmundsson*, 2003], a physical process which can be described as a gravitationally driven flow divergence feedback.

[13] The paper proceeds as follows. The model geometry, equations and boundary conditions are described in section 2. We then describe a steady solution with a mean flow in a given direction (e.g., northward) and a uniform shear in cross-stream direction (e.g., east-west) and write the equations for small perturbations to this mean flow (section 3). The linear stability is analyzed in section 4. The analysis is first performed on a homogeneous (constant coefficients) approximation to the linearized problem in a horizontally unbounded domain (section 4.1) and then to the full linearized equations in a bounded domain (section 4.2). The instability mechanism and the sensitivity to the model parameters are analyzed in section 5, and we conclude in section 6.

2. Model Equations

2.1. Ice Model

[14] The idealized ice sheet we model is two-dimensional and isothermal. The upper ice surface is at $z_s(x, y, t)$ and the base slides over a layer of till at $z_b(x, y)$ (Figure 1). See the notation section for definitions. We assume no vertical shear within the ice itself, effectively assuming that till viscosity is much smaller than the effective ice viscosity so that the vertical shear is concentrated in the till itself [*Macayeal*, 1989], as discussed in section 1. The depth-integrated momentum equations for a steady, low Reynolds number, incompressible and depth-independent ice flow [*Macayeal*, 1989] are then

$$\begin{aligned} \left[2\mu h\left(2\dot{\epsilon}_{xx} + \dot{\epsilon}_{yy}\right)\right]_{,x} + \left(2\mu h\dot{\epsilon}_{xy}\right)_{,y} - \rho g h z_{s,x} - \tau^b_{xz} = 0, \\ \left(2\mu h\dot{\epsilon}_{xy}\right)_{,x} + \left[2\mu h\left(\dot{\epsilon}_{xx} + 2\dot{\epsilon}_{yy}\right)\right]_{,y} - \rho g h z_{s,y} - \tau^b_{yz} = 0, \end{aligned} \tag{2}$$

where $F_{,xi} \equiv \partial F/\partial x_i$, the ice thickness $h \equiv z_s - z_b$ is assumed much smaller than the horizontal scale (although this is not strictly the case in ice stream margins), and $\dot{\boldsymbol{\epsilon}}$ is the ice strain rate tensor,

$$\dot{\epsilon}_{ij} = \frac{1}{2}\left(u_{i,j} + u_{j,i}\right). \tag{3}$$

The ice deforms according to a power law-viscous constitutive relation

$$\boldsymbol{\tau} = 2\mu\dot{\boldsymbol{\epsilon}}, \tag{4}$$

where $\boldsymbol{\tau}$ is the deviatoric stress tensor, and μ is the effective viscosity,

$$\mu = \frac{1}{2} B \dot{\epsilon}_{II}^{\left(\frac{1}{n}-1\right)}. \tag{5}$$

The ice stiffness parameter, B, is assumed constant, $\dot{\epsilon}_{II}^2 = u_{,x}^2 + v_{,y}^2 + u_{,x}v_{,y} + \frac{1}{4}(u_{,y} + v_{,x})^2$ is the second invariant of the strain rate tensor and n is the flow law exponent. The bottom shear stresses τ_{xz}^b and τ_{yz}^b, which couple the ice to the subglacial till, are described in detail in section 2.2.

[15] Mass conservation implies

$$h_{,t} = M - (uh)_{,x} - (vh)_{,y} + \kappa_h\left(h_{,xx} + h_{,yy}\right), \tag{6}$$

where M is the net accumulation rate and the diffusion term can represent thickness diffusion due to snow drift but in fact is introduced to prevent numerical noise, so that κ_h is chosen to have the minimum possible value.

2.2. Till Model

[16] The nature of till rheology is not fully understood. Plastic deformation is consistent with lab experiments and with borehole measurements [*Engelhardt and Kamb*, 1998, 1997; *Engelhardt et al.*, 1990; *Kamb*, 1991; *Tulaczyk et al.*, 2000b], which suggests that to leading order the till failure strength is independent of strain rates [*Tulaczyk et al.*, 2000a, 2000b]. Viscous rheology, on the other hand, predicts till deformation over greater depths, which is consistent with geological observations for most Ross embayment IS, except Whillans ice stream [*Hart et al.*, 1990], and has the potential to explain IS surface structure [*Hindmarsh*, 1998]. *Hindmarsh* [1997] argued that individual till dislocations behave plastically but that the net effect of multiple dislocations on the large scale is effectively viscous.

[17] On the basis of the above arguments we adopt a viscous till rheology in this work. We wish to include the feedback between meltwater production, changed void ratio, and basal friction [*Fowler and Johnson*, 1996, 1995]. For this purpose we assume that the friction applied by the till to the base of the ice sheet may be represented by a simple drag law with a drag coefficient that incorporates the Coulomb-compressive-plastic model introduced by *Tulaczyk et al.* [2000b]. As shown by *Tulaczyk et al.* [2000a], the soil failure strength acting along a given shear plane, τ_f, is determined to leading order by the void ratio, which in turn is determined by the ice pressure acting against the till pore pressure (effective normal stress). The void ratio e, defined as the ratio of pore volume to the volume of till solids, decreases logarithmically as the effective normal stress increases. This implies an exponential dependence between the till failure strength and the void ratio. We therefore let

$$\boldsymbol{\tau}^b = \frac{a\, \mathrm{e}^{-be}}{\langle v \rangle}\mathbf{u}, \tag{7}$$

where $\boldsymbol{\tau}^b = (\tau_{xz}^b, \tau_{yz}^b)$ are the two bottom shear stress components at the ice-till interface, $\mathbf{u} = (u, v)$ the horizontal ice velocity, a and b are constant that depend on the till coefficient of compressibility, internal friction angle and reference values for the effective normal stress and void ratio, and $\langle v \rangle$ is a normalizing velocity scale.

[18] The till void ratio rate of change is assumed proportional to the rate of change of the net available meltwater,

$$e_{,t} = \frac{m_r - d_r}{Z_t}, \tag{8}$$

where m_r is the basal melt rate, d_r is the drainage rate and Z_t is the thickness of the active till layer. Meltwater production is due to heat generation by shear heating due to the friction at the ice-till interface, and due to a geothermal heat flux, G. Heat loss from the till is due to diffusive conduction via the ice and hence should be proportional to the temperature gradient at the base of the ice. In the present isothermal model we account for the heat loss through conduction away from the till layer by using a crude void ratio dissipation term of the form $-\nu e$. An alternative interpretation of this term could be a crude parameterization of loss of water to a subglacial aquifer underlying the till layer (C. Schoof, personal communication, 2007). Basal melt rate is hence determined by the net available heat at the base of the ice [e.g., *Tulaczyk et al.*, 2000b; *Schoof*, 2004],

$$m_r = \frac{1}{L_i \rho}\left(\boldsymbol{\tau}^b \cdot \mathbf{u} + G - \nu e\right), \tag{9}$$

where L_i is the latent heat of fusion. Hence the void ratio rate of change is

$$e_{,t} = \frac{1}{Z_t L_i \rho}\left(\boldsymbol{\tau}^b \cdot \mathbf{u} + G - \nu e\right) - \frac{d_r}{Z_t} + \kappa_e\left(e_{,xx} + e_{,yy}\right), \tag{10}$$

where a diffusion term was introduced for the same numerical reasons as in the case of the continuity equation (6) as well as to crudely represent the horizontal spreading of melt water through the till.

2.3. Boundary Conditions

[19] To close the set of two momentum equations, mass continuity and the equation for the rate of change of the till void ratio, eight boundary conditions are specified on the lateral boundaries. The boundaries parallel to the mean flow are assumed rigid and hence with no normal flow. In order to simplify the analysis, the perturbation shear stress at these boundaries is assumed to vanish (free slip), as well as the normal gradients of thickness and void ratio, implying no diffusive flux of ice or meltwater across the boundary. Our mean flow solution to be described below does have nonvanishing stress and thickness gradients at the boundary, a necessary compromise in order to make the instability analysis tractable. One of our more significant deviations from realism is the assumption that the perturbations to the mean flow are periodic in the direction along the mean flow. As explained in the introduction, this simplifies the analytical analysis of the flow stability, as will be evident in section 3. Our boundary conditions on the boundaries parallel to the mean flow, at $x = 0, L$ are therefore

$$u = 0; \quad h_{,x} = 0 \quad \tau_{xy} = 0; \quad e_{,x} = 0 \tag{11}$$

and at the boundaries perpendicular to the mean flow $y = 0, L$,

$$\begin{aligned} v(x,0) &= v(x,L); \qquad h(x,0) = h(x,L); \\ \tau_{xy}(x,0) &= \tau_{xy}(x,L); \quad e(x,0) = e(x,L). \end{aligned} \tag{12}$$

[20] It is useful to note at this point that while the positive destabilizing feedback here is similar to that used by *Fowler and Johnson* [1995, 1996], there are some important differences. Our formulation includes a time dependence, whereas Fowler and Johnson consider a purely spatial patterning problem in steady state. Also, our periodic boundary conditions do not allow loss of basal water or of ice out of the domain, while Fowler and Johnson deal explicitly with the finite domain size. And finally, our analysis includes the longitudinal stresses neglected by Fowler and Johnson.

3. Linearized Model

[21] The problem involves solving four coupled partial deferential equations (2), (6), and (10), together with the boundary conditions (11) and (12). In this part we linearize the problem, describe the mean field solution and define the perturbation problem to be solved in section 4.

3.1. Linearization

[22] We assume the mean flow to be along one direction (along-flow, y) with shear in the perpendicular direction (transverse, x), and the mean till void ratio to be homogeneous. Hence the fields of interest are decomposed to a mean and perturbation parts as follows

$$\begin{aligned} u &= u'(x,y,t) \\ v &= \overline{v}(x) + v'(x,y,t) \\ h &= \overline{h}(x,y) + h'(x,y,t) \\ e &= \overline{e} + e'(x,y,t) \end{aligned} \tag{13}$$

where an overline denotes the mean fields and prime refers to the perturbation fields. The above linearization implies that the effective ice viscosity is decomposed into a mean and perturbed components, denoted respectively by $\overline{\mu}$ and μ'. It also implies that we do not assume any perturbation in quantities such as G, ν, d_r, or M. Substituting (13) into (2), (6), and (10), we obtain equations for the mean flow by neglecting the perturbations, as well as linearized equations for the perturbations.

3.2. Mean Field Equations and Solution

[23] The equations for the mean fields are

$$\begin{aligned} 0 &= \left(\overline{\mu}\overline{h}\overline{v}_{,x}\right)_{,y} - \rho g \overline{h} z_{s,x} \\ 0 &= \left(\overline{\mu}\overline{h}\overline{v}_{,x}\right)_{,x} - \tau_0 \overline{v} - \rho g \overline{h} z_{s,y} \\ 0 &= M - \left(\overline{v}\overline{h}\right)_{,y} + \kappa_h\left(\overline{h}_{,xx} + \overline{h}_{,yy}\right) \\ 0 &= \tau_0 \overline{v}^2 + G - \nu\overline{e} - d_r L_i \rho + \kappa_e\left(\overline{e}_{,xx} + \overline{e}_{,yy}\right) \end{aligned} \tag{14}$$

where $\tau_0 \equiv a e^{-b\overline{e}}/\langle v \rangle$.

[24] We are interested in finding a mean flow solution with a constant (uniform) shear in the transverse direction, of the form

$$\overline{v} = v_0 + sx. \tag{15}$$

The solution for the other fields that satisfies the mean flow equations (14) is found to be

$$\begin{aligned} \overline{h} &= H_0 + Z_b x, \\ \overline{e} &= e_0, \\ z_s &= H_0 - Z_s y, \\ z_b &= -Z_b x - Z_s y, \end{aligned} \tag{16}$$

where Z_b, Z_s are the slopes of the ice bed and surface respectively, H_0, v_0 and e_0 are constants appearing in the mean thickness, velocity and void ratio, while the parameter s is the mean flow shear. Note that this solution has the bottom sloping in both the x and y directions, as opposed to the usual glaciological situation in which the ice flows down hill. Such a topography is the simplest we have found which supports the specified mean shear flow (15) which is needed to regularize the effective viscosity. While in a flow over frictionless, uniform sloped bed the longitudinal shear stress τ_{xy} is proportional to the across-flow coordinate x [e.g., *Hindmarsh*, 2006a], in this particular case the mean shear stress is the constant $\overline{\tau}_{xy} = B(s/2)^{1/n}$.

[25] Specifying H_0, Z_b, Z_s, and e_0 and plugging (15) and (16) into (14), we find the following constraints on the other parameters required to satisfy the mean equations:

$$s = \frac{\rho g Z_s Z_b}{\tau_0} \tag{17}$$

$$v_0 = \frac{B_0 s Z_b + 2\rho g Z_s H_0}{2\tau_0} \tag{18}$$

$$M = 0 \tag{19}$$

$$G - \nu e_0 - d_r L_i \rho = -\frac{\left(B_0 s Z_b + 2\rho g Z_s (H_0 + Z_b x)\right)^2}{\tau_0} \tag{20}$$

where $B_0 \equiv B(s/2)^{(1/n-1)}$. The first two equations (17) and (18) relate the mean ice velocity to the ice sheet geometry and rheological properties of both the ice and till. The third relation (19) implies zero net mean accumulation, and the last one (20) implies that the mean heat flux out of the till due to geothermal, conduction and drainage processes grows quadratically with x. Note that we have assumed e_0 to be constant above. The spatial dependence on x on the right-hand side of (20) needs therefore to be interpreted as a dependence of the geothermal heating term, G, and/or the drainage component d_r, but not of e_0 for consistency. Setting $Z_s = 3 \times 10^{-3}$, $Z_b = 3 \times 10^{-4}$ and $H_0 = 1800$ m, implies $v_0 \simeq 4.6$ m a^{-1} and $sL \simeq 0.77$ m a^{-1}.

Table 1. Dimensionless Parameters of the Perturbation Equations (26) and (27), (28), (29), and (30) as a Function of the Dimensional Parameters, and Their Numerical Values Based on the Notation Section

Parameter	Value
$S = \frac{1}{2n+1}$	$\simeq 0.166$
$N = 4nS$	$\simeq 1.66$
$H = \frac{b\tau_0 v_0^2 + \nu}{Z_i \rho L_i} \frac{D}{U} \frac{L}{H_0}$	$\simeq 0.3$
$H_\nu = \frac{\nu}{Z_i \rho L_i} \frac{D}{U} \frac{L}{H_0}$	$\simeq 2 \times 10^{-3}$
$F = \frac{\tau_0 L}{\rho g H_0} \frac{U}{D}$	$\simeq 9.6 \times 10^{3}$
$F_e = Fbv_0 \frac{E}{U}$	$\simeq 1.9 \times 10^{4}$
$P = 2nS$	$\simeq 0.83$
$R = B_0 \frac{s}{2} \frac{1}{\rho g H_0}$	$\simeq 1.2 \times 10^{-5}$
$Z = \frac{Z_s}{Z_b}$	$=10$
$A = \frac{D}{U} \frac{v_0}{H_0}$	$\simeq 1.7 \times 10^{-4}$
$K_h = \kappa_h \frac{D}{U} \frac{1}{LH_0}$	$\simeq 1.1 \times 10^{-8}$
$K_e = \kappa_e \frac{D}{U} \frac{1}{LH_0}$	$\simeq 1.1 \times 10^{-10}$

[26] The mean flow solution for the velocities, void ratio and ice thickness satisfies the periodic boundary conditions, although the mean surface elevation and bottom topography do not. The mean flow also satisfies the no-normal flow and no void ratio gradient on the lateral boundaries. Homogeneous boundary conditions are not satisfied by the mean flow as $\overline{h}_{,x} = Z_b$ and $\overline{v}_{,x} = s$, as discussed in section 2.3.

3.3. Perturbation Flow Equations

[27] Given the mean flow solution, we proceed to nondimensionalize the perturbation equations. We introduce the following scales for the fields and coordinates:

$$x^*, y^* = \frac{x}{L}, \frac{y}{L}; \qquad h^* = \frac{h'}{D}; \qquad t^* = \frac{t}{T} \tag{21}$$

$$u^*, v^* = \frac{u'}{U}, \frac{v'}{U}; \qquad e^* = \frac{e'}{E}, \tag{22}$$

where the asterisk denotes dimensionless variables. The problem is linear, and therefore there is an overall scale that is arbitrarily determined. Let this scale be given by the velocity scale U. As a length scale we choose $L = 1000$ km, while D, E and T are set by scaling considerations: The scale D is chosen by balancing the gravitational driving stress forcing with the longitudinal shear stress in the momentum equations. The scale E is chosen by balancing void ratio expansion due to meltwater production and contraction due to heat conduction and shear force, in the void ratio equation. Hence,

$$D = UB_0 \frac{2n+1}{2n\rho g L} \tag{23}$$

$$E = U \frac{2\tau_0 v_0}{b\tau_0 v_0^2 + \nu}. \tag{24}$$

The timescale T is chosen from the mass continuity equation such that the thickness rate of change, $h_{,t}$ is balanced by the perturbation mass advection terms, $\overline{h}u_{,x}$ and $\overline{h}v_{,y}$ so that

$$T = \frac{D}{U} \frac{L}{H_0}. \tag{25}$$

This implies that T is of the order of 10 to 10^2 years (had we scaled T by balancing the time rate of change in the continuity equation with $\overline{v}h_{,y}$ or $u\overline{h}_{,x}$, the time scale would be of the order of 10^6 years and 10^3 years, respectively).

[28] On the basis of the above, the linearized dimensionless perturbation problem is

$$\begin{aligned}
0 &= N\delta_h u_{,x} + P\delta_h v_{,y} + (1 + \delta_h x) \\
&\quad \left(Nu_{,xx} + Su_{,yy} + v_{,xy} - h_{,x}\right) + Dh_{,y} - Fu \\
0 &= S\delta_h v_{,x} + (1 + \delta_h x)\left(u_{,xy} + Sv_{,xx} + Nv_{,yy} - h_{,y}\right) \\
&\quad + Dh_{,x} + Z\delta_h h + S\delta_h u_{,y} \\
&\quad + (1 + \delta_v x)F_e e - Fv \\
h_{,t} &= -\delta_h u - (1 + \delta_h x)\left(u_{,x} + v_{,y}\right) - A(1 + \delta_h x)h_{,y} \\
&\quad + K_h\left(h_{,xx} + h_{,yy}\right) \\
e_{,t} &= (1 + \delta_v x)Hv - He - (H - H_\nu)(2 + \delta_v x)\delta_v x e \\
&\quad + K_e\left(e_{,xx} + e_{,yy}\right)
\end{aligned} \tag{26}$$

where the * were dropped, $\delta_h = Z_b L/H_0$, $\delta_v = sL/v_0$ and where the value of the capitalized dimensionless coefficients is shown in Table 1 in terms of the dimensional quantities.

[29] This set of equations, which involves nonconstant coefficients, is solved numerically in section 4.2 with the proper boundary conditions, as specified in section 2.3. Yet it turns out to be useful to first analyze an approximate form. First, the fact that $\delta_h \sim \delta_v \ll 1$ implies that all coefficients in (26) may be assumed spatially constant, which is essentially the quasi-uniform flow approximation [*Hindmarsh*, 2004b]. Second, we have carefully examined the magnitude of each of the terms in the equations (26) and found that the dominant terms for a wide range of parameters are those involving the coefficients S, N, H, F and F_e only. This leads to a much simpler form of the linear perturbation problem,

$$0 = Nu_{,xx} + Su_{,yy} + v_{,xy} - h_{,x} - Fu \tag{27}$$

$$0 = u_{,xy} + Sv_{,xx} + Nv_{,yy} - h_{,y} + F_e e - Fv \tag{28}$$

$$h_{,t} = -u_{,x} - v_{,y} \tag{29}$$

$$e_{,t} = Hv - He \tag{30}$$

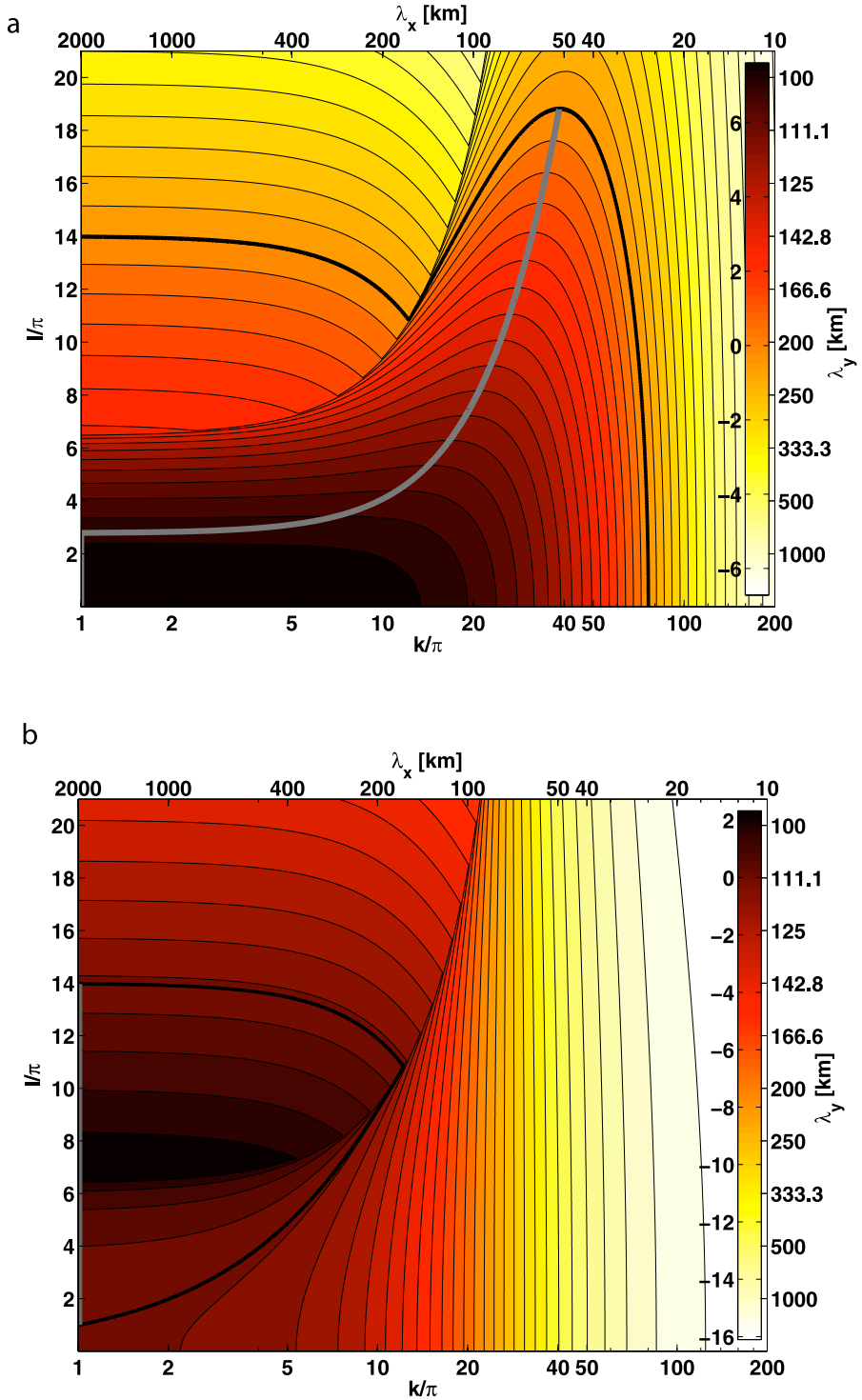

Figure 2. The infinite domain, constant coefficient approximation to the growth rates (a) $\Im(\omega_+)$ and (b) $\Im(\omega_-)$ in ka^{-1} as function of the wave numbers k, l for $F \simeq 9672$, $F_e \simeq 19{,}206$, $n = 2.5$ and $H \simeq 0.306$. The thick black curves are the neutral curves, and the gray curves mark the maximum growth rate at a constant l.

which is solved in the first part of section 4. The approximate form of the linear problem allows us to derive an analytic expression for the rate of growth of small perturbations. We then further justify this approximation below by comparing its results to the numerical solution of the fuller equations. It is also interesting to note that had we used a regularization of an effective viscosity μ (e.g., $\mu = B[\dot{\epsilon}^2 + d_0^2]^{(1-n)/2n}/2$) instead of using a nonzero mean shear

as done here, the resulting equations would be similar to our (27)–(30) (C. Schoof, personal communication, 2007).

4. Linearized Stability Analysis

[30] In this section we solve the linear perturbation problem derived in section 3. We first present an analytic solution to the approximated form of the perturbation problem (27), (28), (29), and (30) in an unbounded domain. We then solve numerically the full linear equations with the nonconstant coefficients (26), and in a laterally bounded domain with the boundary conditions (11) and (12). We show that the approximate unbounded solution predicts very accurately the eigenmodes of the exact solution, up to the quantization of the eigenmodes induced by the boundaries.

4.1. Constant Coefficients in an Unbounded Domain Approximation

[31] The system (27), (28), (29), and (30) in an unbounded domain has a plane wave solution of the form

$$\mathbf{F}_{\mathrm{ub}}(x,y,t) = \boldsymbol{\xi}_{\mathrm{ub}} \mathrm{e}^{i(kx+ly-\omega t)} \tag{31}$$

where $\mathbf{F}_{\mathrm{ub}} = (u,\ v,\ h,\ e)^{\mathrm{T}}$, $\boldsymbol{\xi}_{\mathrm{ub}}$ is a vector of constant coefficients, k and l are the wave numbers corresponding to the x (transverse) and y (along-flow) directions respectively, and the imaginary part of the frequency, $\Im(\omega)$, is the growth rate. Only two out of the four equations in (27), (28), (29), and (30) are prognostic (time-dependent), and hence the solution for the growth rate can be reduced to that of a two by two linear system:

$$\begin{pmatrix} \alpha(k,l)+i\omega & \beta(k,l) \\ \gamma(k,l) & \delta(k,l)+i\omega \end{pmatrix} \begin{pmatrix} e_o \\ h_o \end{pmatrix} = \mathbf{0}.$$

The functions α, β, γ and δ depend on the wave numbers k and l and on the dimensionless coefficients and are either real or imaginary,

$$\alpha = -\frac{F_e H}{\phi - \psi l^2} - H, \tag{32}$$

$$\beta = i\frac{(l+\psi l)H}{\phi - \psi l^2}, \tag{33}$$

$$\gamma = i\frac{(l+\psi l)F_e}{\phi - \psi l^2}, \tag{34}$$

$$\delta = \psi + \frac{(l+\psi l)^2}{\phi - \psi l^2}, \tag{35}$$

where $\phi(k,l) = -(F + k^2 S + l^2 N)$ and $\psi(k,l) = -k^2(F + k^2 N + l^2 S)^{-1}$. The growth rate is given by the two solutions

$$\Im(\omega_{\pm}) = \frac{1}{2}\left\{(\alpha+\delta) \pm (\alpha-\delta)\Re\sqrt{1+\frac{4\beta\gamma}{(\alpha-\delta)^2}}\right\} \tag{36}$$

and is shown in Figure 2 as a function of the two wave numbers.

[32] Both solutions give rise to unstable modes in a partially overlapping k, l regime for seemingly reasonable parameter choices. However, the maximum growth rate at a given l obtained from the solution $\Im(\omega_-)$ is smaller than the one obtained by $\Im(\omega_+)$ for all l, as shown in Figure 3. On this basis we limit the discussion in the following sections to the larger growth rate solution $\Im(\omega_+)$.

[33] The solution $\Im(\omega_+)$ is seen to be unstable at long transverse wavelengths ($k \to 0$) but stable at short transverse wavelengths ($k \to \infty$) (Figure 2a). The maximum growth rate for values of the long-flow wave number l above a certain threshold ($l/\pi \quad 3$) occurs at an intermediate transverse wave number, thereby demonstrating a scale selective instability. However, the global maximum of the growth rate occurs at infinitely long waves (both k and l approaching zero). These features as well as other properties of the instability mechanism will be analyzed and discussed in sections 5 and 6.

4.2. Laterally Bounded Domain

[34] Next, we solve the full linear perturbation system with nonconstant coefficients (26), imposing the boundary conditions specified by (11) and (12). Assuming a solution of the form,

$$\mathbf{F}_{\mathrm{full}}(x,y,t) = \boldsymbol{\xi}_{\mathrm{full}}(x) \mathrm{e}^{i(ly-\omega t)} \tag{37}$$

where $\mathbf{F}_{\mathrm{full}} = (u,\ v,\ h,\ e)^{\mathrm{T}}$ and where $\boldsymbol{\xi}_{\mathrm{full}}(x)$ is a vector of eigenfunctions to be calculated, reduces (26) to a system of four second-order ordinary differential equations (ODEs) for u, v, h and e, with nonconstant coefficients, and with l and ω as parameters. Alternatively, this system of second order ODEs can be represented as a set of first-order ODEs of the form

$$\mathbf{Y}_{,x} = \mathbf{B}(x,l,\omega)\mathbf{Y} \tag{38}$$

where

$$\mathbf{Y} = \left(u, v, h, e, u_{,x}, v_{,x}, h_{,x}, e_{,x}\right)^{\mathrm{T}} \tag{39}$$

and where $\mathbf{B}$ is an eight by eight matrix. We solve this boundary value problem using the MATLAB *bvp4c* solver. Once the along-flow wave number, l, is specified, this problem involves solving for eight coefficients and one parameter, ω, which requires nine additional conditions. The boundary conditions of the original problem include eight equations (11) and (12), and one additional constraint comes from specifying the otherwise arbitrary overall scale for the linear solution, by setting the value of $h(x = 0)$.

[35] Figure 4 shows the numerical solution for the growth rate $\Im(\omega)$ calculated as function of the transverse wave number k (pluses), together with the analytic solution (lines) of the constant coefficient unbounded domain approximation (36), for three different values of the along-flow wave number, l. Note that the transverse wave number does not appear in the full linear equations solved by the boundary value problem solver, and that the pluses in Figure 4 are calculated as function of k as follows. The solver is

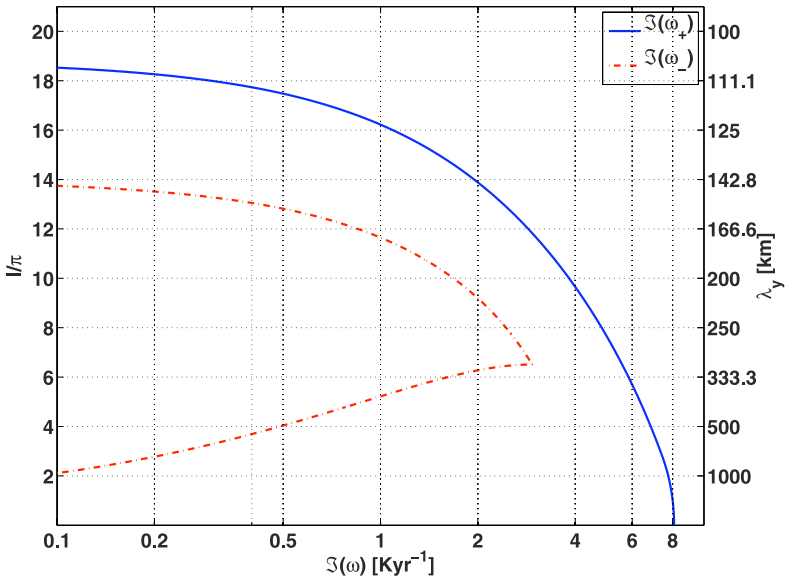

Figure 3. The maximum growth rate $\Im(\omega_{\pm})$ in ka^{-1} (horizontal axis) for a given value of the along-flow wave number l for all values of the transverse wave number k, as function of the along-flow wave number l (vertical axis). Both solutions are drawn, using the unbounded domain, constant coefficient approximation (36) for $F \simeq 9672$, $F_e \simeq 19{,}206$, $n = 2.5$ and $H \simeq 0.306$. This demonstrates that $\Im(\omega_+) > \Im(\omega_-)$ for all l.

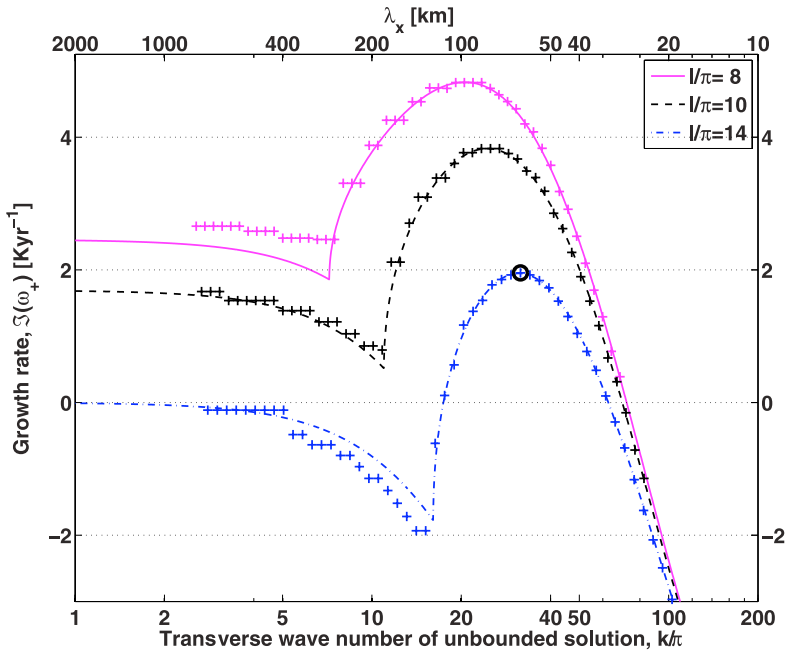

Figure 4. The growth rate $\Im(\omega_+)$ in ka^{-1}, calculated numerically for the full linear problem with nonconstant coefficients in a bounded domain (pluses) and the unbounded domain analytic solution (lines) as a function of the k wave number of the unbounded domain solution for $l/\pi = 8$, 10, 14, which correspond to dimensional along-flow wavelengths of 250, 200, and ~143 km, respectively. Mode quantization is clearly seen at low transverse (cross-flow) wave numbers. The eigenfunctions of the most unstable mode for $l/\pi = 14$ (circle) are shown in Figure 5.

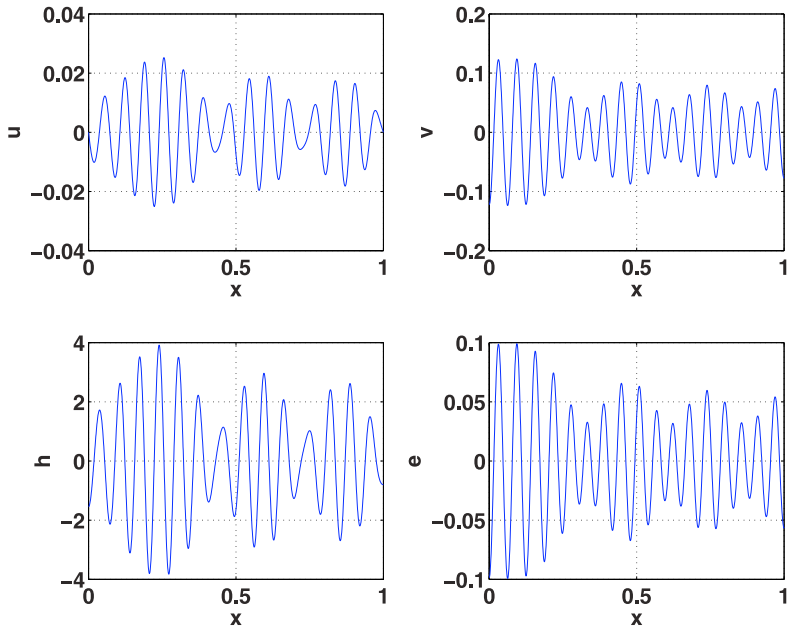

Figure 5. The eigenfunctions u, v, h, and e, of the most unstable mode obtained from the solution of the full linear problem, for dimensional along-flow wavelength of ∼143 km ($l/\pi = 14$, marked by the circle in Figure 4).

initialized with the spatial structure and the eigenvalue ω of the solution to the constant coefficient problem for a specified value of the transverse wave number k. The resulting eigenvalue of the full problem is then plotted as function of this wave number k.

[36] The boundary value problem solution clearly agrees well with the approximate analytic solution. A mode quantization is apparent in the boundary value problem solution as a grouping of the frequencies into discrete values, especially at long wavelengths, as is typical of eigenvalue problems in a bounded regime [*Haberman*, 2004, p. 42].

[37] Figure 5 shows the spatial structure of the eigenfunctions u, v, h and e at $t = 0$, $y = 0$, obtained by solving the full nonconstant coefficient problem in a bounded solution, and corresponding to the most unstable mode for $l/\pi = 14$. While the eigensolutions of the unbounded solution are simply sines and cosines, the eigenfunctions of the full problem are only quasiperiodic in space, due to the presence of inhomogeneities (nonconstant coefficients) in the full problem. As expected, the average wavelength of the bounded solution eigenfunctions is similar to the wavelength of the analytic solution from which it was obtained using the initialization procedure explained above.

5. Discussion

5.1. Instability Mechanism

[38] We see a good agreement between the numerically calculated growth rates of the linear problem with nonconstant coefficients (26) and those of the linear constant coefficient approximation in an unbounded domain (27), (28), (29), and (30), as demonstrated by Figure 4. This agreement suggests that the constant coefficient approximation, including both making the quasi-uniform flow approximation and dropping other small terms, is indeed consistent in the sense that the simpler constant coefficient equations reproduce the results of the fuller ones. We therefore study the instability mechanism by analyzing the growth rate solution (36) of the constant coefficient unbounded domain approximation.

[39] In this section we analyze the distribution of unstable modes as a function of the wave numbers (or equivalently wavelengths) in the (transverse, along-flow) directions, (k, l), and discuss the instability mechanism. We distinguish between short, intermediate, and long transverse wavelengths.

[40] The main source of instability at all transverse wavelengths is the weakening of the bottom friction by meltwater production [e.g., *Tulaczyk et al.*, 2000a, 2000b; *Fowler and Johnson*, 1996, 1995]. Momentum dissipation through basal friction results in heating and production of meltwater; the resulting increase of the till void ratio weakens the till and hence reduces the resistance to ice sliding and accelerates the flow. This leads to more basal heating, melting and further increase in the void ratio, and therefore to a positive feedback which results in an instability. We will shortly see that for values of the along-flow wavelengths $\lambda_y = 2\pi/l$ below 500 km or so, the instability growth rate as function of the transverse wavelength $\lambda_x = 2\pi/k$ peaks for a range of transverse wavelengths that roughly coincide with observed widths of pure ice streams. This points to the existence of stabilizing feedbacks at long and short transverse wavelengths, which we now discuss.

[41] At long transverse wavelengths, stability occurs through a mechanism we can describe as a gravitationally driven flow divergence feedback. This refers to the coupling of the driving pressure gradient in a given direction due to the surface slope (e.g., $-gh_y$ in the dimensional form of

equation (28)), and the mass flux divergence in the same direction (e.g., $H_0 v_y$ in the dimensional form of equation (29)). The surface slope creates a horizontal pressure gradient which drives a flow, and the driven flow divergence then acts to eliminate the surface slope and stabilize the flow. This negative feedback is active in both horizontal directions and is dominant at long but not infinite wavelengths. The growth rate at long transverse wavelengths is given by

$$\Im(\omega_+)_{k\to 0} \approx \frac{1/2}{F + l^2 N}\left(H(F_e - F) - l^2 NH - l^2\right). \qquad (40)$$

The third term on the right-hand side of (40) is the dominant stabilizing term which represents the gravitationally driven flow divergence feedback due to the two components mentioned above. The dependence on $-l^2$ in the growth rate, indicates that this stabilizing feedback is nothing but the Nye diffusion [*Nye*, 1960, 1959; *Gudmundsson*, 2003] which is derived from a similar combination of a bottom sliding law and the mass continuity equation. Clearly, the sign of the growth rate depends on the right-hand side of (40). In the case when $F_e > F$ the first term is always positive which means that the diffusion terms in (40) determine the stability. However, when $F_e < F$ the growth rate is always negative.

[42] At short transverse wavelengths, momentum dissipates through longitudinal stress gradients, as demonstrated by *Hindmarsh* [2006b] for $n = 1$. Beyond some transverse wavelength, this mechanism stabilizes the flow completely. The growth rate at short transverse wavelengths is given by

$$\Im(\omega_+)_{k\to\infty} \approx H\left(\frac{F_e}{F + k^2 S + l^2 N} - 1\right). \qquad (41)$$

As $k \to \infty$, the first term in the parentheses vanishes, leaving the growth rate equal to the negative and therefore stable $-H$. This stabilizing mechanism is somewhat unusual and therefore interesting. Typically, viscosity terms in Newtonian fluids at higher Reynolds numbers, with time derivatives included in the momentum equations, result in a growth rate that is proportional to the negative of the wave number squared ($\propto -k^2$). However, in the low Reynolds number case of a Stokes flow, where the momentum equations are diagnostic (no time derivatives), the effect of the viscosity is combined with that of the prognostic (time-dependent) equations. Specifically, the stabilizing $-H$ term in (41) results from the term $-He$ in the void ratio equation representing reduction of basal heat dissipation and heat loss through conduction from the ice sheet base (or in the alternative interpretation of $-\nu e$ in (9), loss of water to a deeper aquifer).

[43] At long wavelengths, basal friction dominates momentum dissipation, and via the induced basal melting results in a destabilizing feedback. As the transverse wave number k increases, the longitudinal stress terms in the linearized equations (Nu_{xx} in (27) and Sv_{xx} in (28)) which represent momentum dissipation via horizontal momentum diffusion, become increasingly dominant. For large enough k (short wavelengths), the strong induced velocity contrasts result in large longitudinal and lateral stresses which grow like k^2. Because no available stresses due to other terms in the equations can provide balance, the perturbation ice velocities become smaller and smaller. The vanishing velocities weaken the destabilizing basal friction heating (Hv in (30)), making the void ratio decrease via a reduction in the heat dissipation and conduction ($-He$ in (30)), which remains the only significant term on the right-hand side of this equation. Hence the above asymptotic result for the growth rate at the limit of infinite k.

[44] The instability growth rate does not vanish at very large scales, when both (k, l) vanish, but rather it has a maximum. This implies that the most unstable mode has no spatial structure associated with it, as was the cases of *Hindmarsh* [2006b, 2004a], *Clarke et al.* [1977], and *Nye and Robin* [1971]. It is not clear whether this behavior is physical; it does not occur at all parameter regimes in this study (see case $F > F_e$ below) and is perhaps due to the oversimplifications involved in our model formulation. This is further discussed in section 6.

[45] However, for along-flow perturbation wavelengths ($2\pi/l$) above about 300 km in Figure 2a, the rate of growth has a maximum for an intermediate transverse wavelength ($2\pi/k$) that roughly corresponds to the width of observed pure ice streams. This preferential growth at an intermediate wavelength is encouraging, and may indicate that the simple model here contains some of the elements that lead to the determination of the width of observed ice streams. Now, we note that the along-flow wavelength of the perturbation cannot take values larger than the basin length in the along-flow direction. We therefore conclude that for a finite domain size in the along-flow direction, the model displays preferential growth at a wavelength roughly corresponding to the width of ice streams. The maximum growth rate at intermediate transverse wavelengths is found at even longer along-flow wavelengths $2\pi/l$ (and hence for longer domain size in this direction) for other parameter choices (section 5.2). The physics we find here for the preferential growth at an intermediate wave length is, of course, the selective dissipation of short waves by longitudinal stress gradients and of long waves by the Nye diffusion, or equivalently the gravitationally driven flow divergence feedback discussed above.

[46] The criterion for stability in infinitely long along-flow and transverse wavelength (both k, $l \to 0$) is that

$$F > F_e, \qquad (42)$$

where we note again that F is the nondimensional bottom friction coefficient and F_e represents the weakening of the bottom friction due to the meltwater effect. The physical interpretation of this condition is simply that the model is unstable at long wavelengths when the destabilizing positive feedback due to the meltwater production overcomes the bottom friction. The gravitationally driven flow divergence feedback (that is, the Nye diffusion) relies on both anomaly pressure gradients and anomaly divergence, both of which vanish at the limit of both k, $l \to 0$. Therefore this mechanism cannot stabilize the flow at the large wavelength limit, and the remaining mechanism of bottom friction is the only way to achieve such a stabilization, as indicated by (42). When (42) is satisfied the unstable modes are confined in a regime of small (but nonzero) along-flow wave number and small (including zero) transverse wave

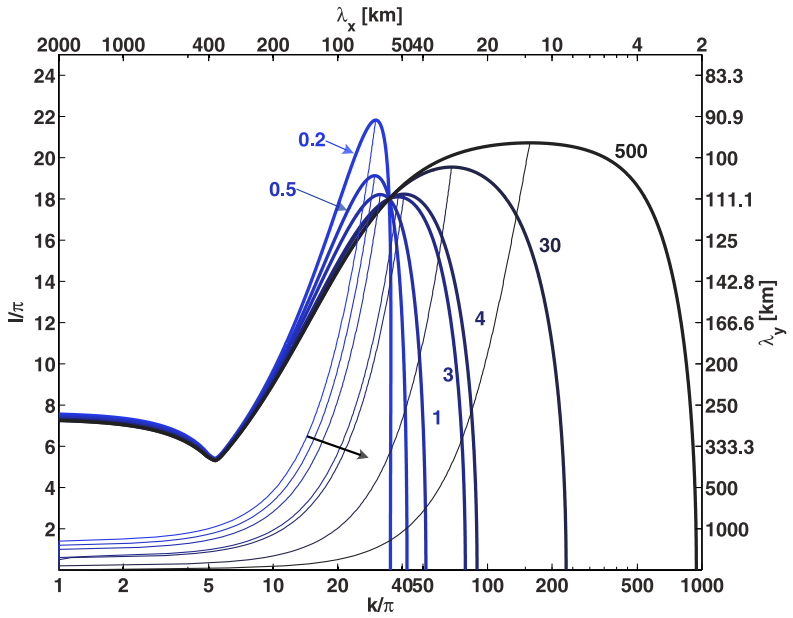

Figure 6. The unstable domain as function of both wave numbers, shown by the neutral curve $\Im(\omega_+) = 0$, for different values of Glenn's law exponent n. The thick lines mark the neutral curves for a range of n values, and the thin lines correspond to the transverse wave number k_m of the most unstable mode for a constant l. The arrow points in the direction in which the thin lines mark growing values of n. Note there is no qualitative difference between Newtonian ($n = 1$) and non-Newtonian fluids.

number (see Figures 7 and 8). In this case there are values of l for which the most unstable mode is associated with nonzero transverse wave number but the globally most unstable mode has $k = 0$, so that it has no transverse structure.

[47] We therefore find an instability mechanism, as well as interesting preferential growth at an intermediate transverse wavelength due to stabilizing feedbacks that stabilize the flow for both short and long transverse wavelengths.

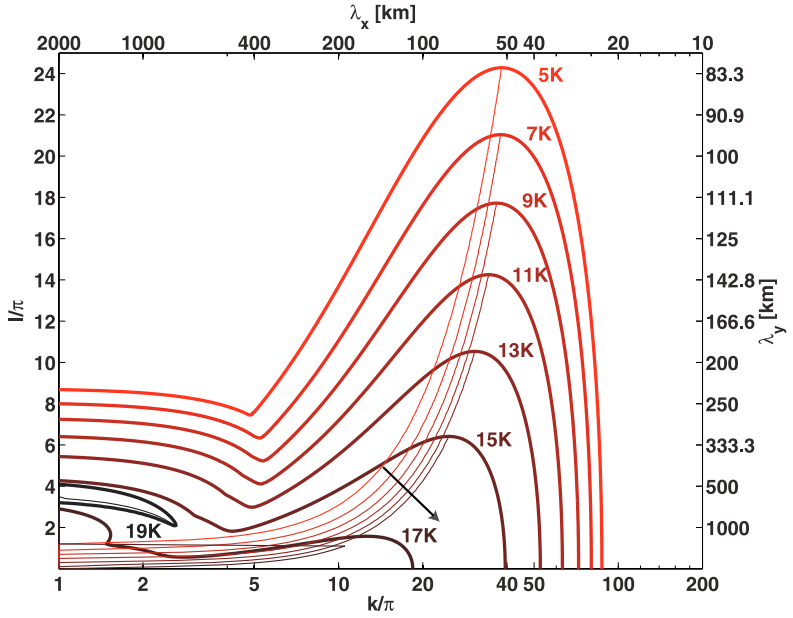

Figure 7. The unstable domain as function of both wave numbers, shown by the neutral curve $\Im(\omega_+) = 0$, for different values of the dimensionless number F. The thick lines mark the neutral curves for a range of F values, and the thin lines correspond to the transverse wave number k_m of the most unstable mode for a constant l. Each curve is marked by the corresponding values of F in units of $K = 1000$. The arrow points in the direction in which the thin lines mark growing values of F. The curve ($F = 19{,}000$) is the neutral curve that results from satisfying the condition $F > F_e$ (42); see text.

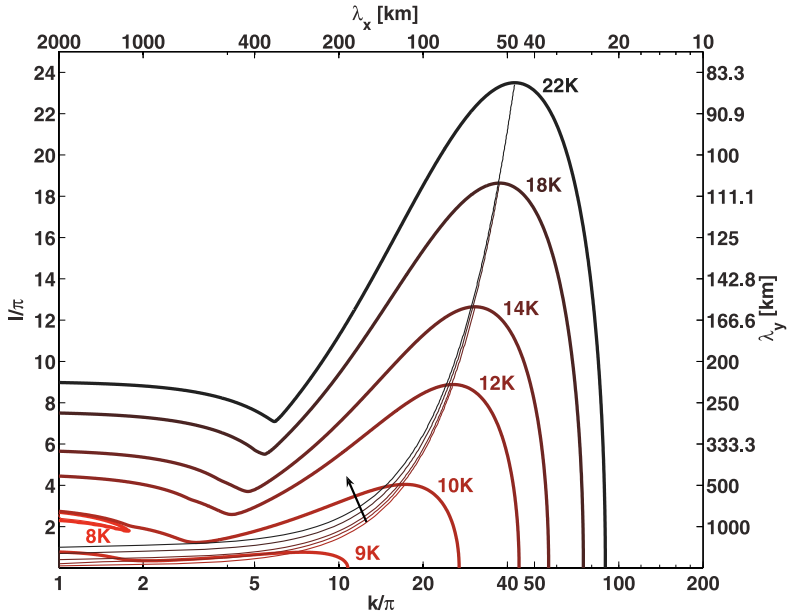

Figure 8. The unstable domain as function of both wave numbers, shown by the neutral curve $\Im(\omega_+) = 0$, for different values of the dimensionless number F_e. The thick lines mark the neutral curves for a range of F_e values, and the thin lines correspond to the transverse wave number k_m of the most unstable mode for a constant l. Each curve is marked by the corresponding values of F_e mark in units of $K = 1000$. The arrow points in the direction in which the thin lines mark growing values of F_e. The curve ($F_e = 8000$) is the neutral curve that results from satisfying the condition $F > F_e$ (42); see text.

The growth rate of the perturbations depends on the choices for the model parameters, but we can find model parameters for which the growth rate is of the order of hundreds of years. See, for example, the growth rate in Figure 2a around a transverse wavelength of $\lambda_x = 75$ km and along flow wavelength of $\lambda_y = 180$ km, which is equal to $\Im(\omega) \approx 3$ ka, which translates into a dimensional growth timescale of $1/\Im(\omega) \approx 330$ years. It should be noted that the growth rates found here are perhaps still too slow to account for the observed switching on and off of the Antarctica ice streams which seem to occur on a timescale of hundred(s) of years.

5.2. Sensitivity to Parameters

[48] The solution (36) for the growth rate in the unbounded constant coefficient linear perturbation case (equations (27), (28), (29), and (30)), involves four dimensionless independent parameters, F, F_e, H and n (Table 1). In this section we analyze the sensitivity of this approximate solution to these four parameters. We find that generally the unstable domain in the wavelengths space is not overly sensitive to the different model parameters. In particular, the solution is not qualitatively difference for a Newtonian fluid, when the Glenn's law exponent is set to $n = 1$, indicating that shear thinning does not play a significant part in the instability seen in this paper.

[49] Consider first the sensitivity to n, the exponent in the effective ice viscosity (5). Figure 6 shows that the unstable area changes quantitatively but not qualitatively as n varies through several orders of magnitude. In particular, the qualitative shape of the unstable domain and the general instability mechanism are unchanged when ice is treated as a Newtonian fluid ($n = 1$). This implies that shear thinning does not play a major role in our results, in spite of the related positive feedback mentioned in the introduction: a small perturbation to the flow which enhances the strain rates leads to a weakening of the effective viscosity, and this, in turn, leads to a further increase in the perturbation velocity and therefore to a positive feedback.

[50] As the ice flow law tends to be more plastic (large values of n), the strength of longitudinal shear stresses declines, and hence so does their effect as stabilizers at short transverse wavelengths. This results in the expansion of the unstable domain further into shorter transverse wavelengths and in a decreased scale of the most unstable modes (Figure 6). However, the effect of meltwater spreading in the till (represented by the term $\kappa_e \nabla^2 e$ in (10)) grows with the wave number like k^2. Consequently, stability recovers as the water lubrication is increasingly smeared within the till (K_e in 26) as the wavelength gets shorter. This resembles the negative hydraulic feedback of *Fowler and Johnson* [1995].

[51] The parameter F appears in both momentum equations (27) and (28), and accounts for nonscale-selective momentum dissipation by bottom friction. As F increases, so does the momentum dissipation and hence the area of the unstable domain in the wavelengths plane reduces (Figure 7). Since momentum dissipation through bottom friction is larger as F increases, less is dissipated by longitudinal stresses at a particular along-flow wavelength. This implies that at that particular along-flow wavelength the stabilizing effect of longitudinal stresses reduces and hence that the most unstable mode shifts to a shorter transverse wavelength with respect to a smaller F. This shift is clearly shown by the thin curves in Figure 7.

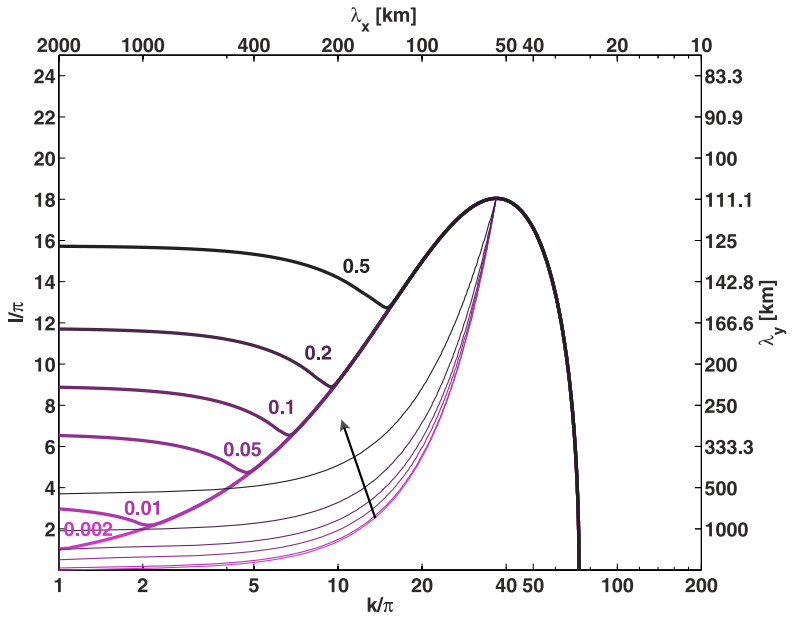

Figure 9. The unstable domain as function of both wave numbers, shown by the neutral curve $\Im(\omega_+) = 0$, for different values of the dimensionless number H. The thick lines mark the neutral curves for a range of H values and the thin lines correspond to the transverse wave number k_m of the most unstable mode for a constant along the flow wave number l. The arrow points in the direction in which the thin lines mark growing values of H.

[52] The parameter F_e appears in the along-flow momentum equation (28) and also originates from bottom friction. This parameter, though, represents the positive feedback between melt water production by shear heating at the ice-till interface and flow velocity. Consequently the unstable zone in the (k, l) plane expands with increasing F_e (Figure 8). The wave number k_m of the most unstable mode reduces as F_e increases for a similar reason to that analyzed above for the sensitivity to F, although in this case the response is weaker at long and intermediate along-flow wavelengths.

[53] As mentioned in section 5.1, the magnitude of F relative to that of F_e has a critical effect on the stability due to their opposite effects. In particular, as $F_e - F$ approaches zero from above, the unstable regime contracts toward the origin of the (k, l) space, leaving only the very long waves to be unstable (highest F contour in Figure 7 and lowest F_e contour in Figure 8). When $F_e - F < 0$, the model is stable for k, l approaching zero (infinitely long wavelengths). The unstable domain is then confined to a small region with finite values of l. The most unstable mode in this case has $k = 0$ and $l \neq 0$.

[54] The final dimensionless number, H, scales the void ratio rate of change (30). An increase of H implies a faster response of the void ratio rate of change to variations of net meltwater in the ice-till interface. This has a prominent effect on the neutral curve at long transverse wavelengths, since H affects the destabilizing processes at the ice-till interface but does not affect the gravitationally driven flow divergence feedback (Figure 9). Consequently, a decrease in H increases the stability of modes with long wavelengths, as clearly shown by the drift of the neutral curve at long transverse wavelengths to long along-flow wavelengths, until it converges into a bell shaped curve (the curve $H = 0.002$ in Figure 9) when $H \leq H_c(l)$, where

$$H_c(l) = \left[\frac{l\left(\sqrt{F + l^2 N} - \sqrt{F_e}\right)}{F - F_e + l^2 N}\right]^2. \tag{43}$$

The effect of H on long wavelengths is also evident by the drift of the curves of most unstable modes to longer along-flow wavelength as H decreases. The neutral curve at long transverse wavelengths is quite sensitive to variations in H. The response of both the most unstable modes and of the extent of the unstable area at short transverse wavelengths are more sensitive to n.

[55] In summary, our finding that shear thinning $n > 1$ does not a play a significant role in the instability, as well as the existence of instability at very long wavelengths, may be due to the restrictive nature of our model and analysis, including two factors in particular: first, the assumed linear mean shear, and second, the linearized perturbation analysis. We cannot rule out that shear thinning may play a role in an instability if the mean shear were not linear (i.e., nonuniform shear), or if we considered finite amplitude weakly nonlinear effects. Both of these extensions may result in a more prominent role of the shear thinning feedback as follows. With shear thinning acting to further destabilize the short waves, one could stabilize the very long wavelengths using one of the nonscale selective friction processes (e.g., bottom friction, via the F parameter). This may leave the intermediate wavelengths unstable, possibly at wave lengths consistent with the observed width of ice streams. This is clearly a very speculative suggestion at this point.

[56] The scale selection we find here in the cross-stream direction occurs, as we have seen, only when $l \neq 0$. The scale selection for $l \neq 0$ is interesting, yet does not seem satisfactory as an explanation for observed ice stream widths. A finite domain size (in the downstream (y) direction, without the periodic boundary conditions) will ultimately be a better way of understanding transverse wavelength selection.

6. Conclusions

[57] The linearized stability of shear ice flow over a homogeneous porous till layer was studied using an idealized ice sheet model in two horizontal dimensions that includes longitudinal stresses and a bottom sliding feedback. The results of a linear stability analysis suggest that such a configuration may be inherently unstable. The potential implication is that pure ice streams, such as those at Siple coast, west Antarctica, may possibly be the results of a spontaneous instability of ice flow, which would be consistent with their observed decoupling from specific topographic features in Antarctica.

[58] The growth rate was calculated (1) analytically as function of the two horizontal wavelengths in the limit of an unbounded domain and neglecting all spatially varying coefficients in the governing linearized equations and (2) numerically in the fuller case of variable coefficients and a bounded domain. An agreement between the two methods was demonstrated. The main source of instability is the weakening of the basal friction. Momentum dissipation through basal friction and heating results in the production of meltwater. The resulting increase of the till void ratio weakens the till [*Tulaczyk et al.*, 2000a, 2000b] and hence reduces the resistance to ice sliding, accelerates the flow and therefore leads to a positive destabilizing feedback [*Fowler and Johnson*, 1996, 1995].

[59] For a finite domain size, the instability growth rate as function of the transverse (cross-flow) wavelength peaks for a range of transverse wavelengths that roughly coincide with the observed widths of pure ice streams. This implies stabilizing mechanisms at both short and long transverse wavelengths which we have analyzed in detail. At short transverse wavelengths, longitudinal stress gradients stabilize the flow, acting as a scale-selective dissipation mechanism [*Hindmarsh*, 2006b]. At long transverse wavelengths stability occurs through the Nye diffusion mechanism [*Nye*, 1959; *Gudmundsson*, 2003] that can be described as a gravitationally driven flow divergence feedback. This involves a horizontal pressure gradient due to a surface slope driving a flow, and the flow, in turn, acting to eliminate the driving surface slope. The selection of intermediate unstable wavelengths occurs, however, only for certain parameter and perturbation structure choices. The stabilizing feedbacks found here are different from the one analyzed by *Fowler and Johnson* [1996, 1995], although the instability mechanisms are fundamentally similar.

[60] The instability and its mechanism were found to be robust to changes in the problem parameters. In particular, the instability does not change qualitatively as the ice flow law is assumed Newtonian ($n = 1$), implying that shear thinning does not play a role in the instability analyzed here. We did not rule out the possibility that shear thinning enhances the instability of ice flow and leads to ice stream formation based on the shear thinning feedback discussed in the introduction. Furthermore, one expects shear thinning to preferentially amplify the instability at short wavelength, as perturbations with a small spatial scale would be characterized by a larger perturbation to the strain rates. That this process does not play a role here is perhaps due to the restrictive nature of our model and analysis. In particular, we assume that the mean shear is uniform (that is, the velocity amplitude is linear in the cross flow distance). Using a nonuniform mean shear would allow additional terms to enter the perturbation equations and perhaps represent additional shear thinning effects in a way that would lead to an instability. It is also possible that shear thinning enters via a weakly nonlinear effect excluded by our linearized analysis. Thus we feel that the role of longitudinal shear stresses and of shear thinning in particular should be further investigated by not making the above restrictive assumptions.

[61] While we are able to obtain some interesting qualitative understanding of some potential instability mechanisms that may be relevant to the formation of pure ice streams, it is important to keep in mind that the model analyzed here is, intentionally, very simple. As a result, although we find that the instability is robust to the model parameters, we still cannot determine if this instability mechanism is relevant to the actual present or past ice sheets and can lead to the spontaneous generation of pure ice streams. In particular, two main features of our analysis results prevent us from being able to attribute the development of actual pure ice streams to the instability mechanism discussed here. First, for most parameter values, the instability is maximal at infinitely long wavelengths, $(k, l) \rightarrow 0$. Second, the growth rates found here are of the order of hundreds of years, and therefore perhaps too slow to account for the observed switching on and off of the Antarctic ice streams. This study, therefore, can only point to an ice flow instability as a speculative potential mechanism for the spontaneous generation of pure ice streams.

Notation

B	$\simeq 70$ MPa $s^{1/n}$, ice stiffness.
B_0	$= B(s/2)^{[(1/n)-1]}$.
D	ice thickness perturbation scale.
E	void-ratio perturbation scale.
F, F_e, H, $S(n)$, $N(n)$	dimensionless parameters of unbounded perturbation problem.
G	geothermal heating, equal to 0.07 W m^{-2}.
H_0	ice mean thickness at origin, equal to 1800 m.
L	characteristic length scales, equal to 1000 km.
L_i	latent heat of fusion, equal to 333.5 kJ kg^{-1}.
M	ice net accumulation.
T	timescale.
U	velocity perturbation scale.
Z_t	active till thickness, equal to 1.8 m.
(Z_s, Z_b)	surface, bottom slopes, equal to $(3,0.3) \times 10^{-3}$.

a	till strength coefficient, equal to 3776 MPa.
b	till strength exponent, equal to 20.
d_r	meltwater drainage rate.
e	till void ratio.
e_0	ice mean till void ratio, equal to 0.56.
g	gravitational acceleration, equal to 9.81 m s^{-2}.
h	ice thickness.
(k, l)	x, y (transverse, along-flow) wave numbers.
k_m	transverse wave number of the most unstable mode for a constant l.
m_r	basal melt rate
n	ice flow law exponent, equal to 2.5.
s	ice mean velocity shear.
t	time.
(u, v, w) or (u_1, u_2, u_3)	ice velocity vector.
v_0	ice mean velocity at origin
$\langle v \rangle$	normalizing velocity scale, equal to 5 m a^{-1}.
(x, y, z) or (x_1, x_2, x_3)	position vector.
z_s, z_b	surface, bottom topography.
$\alpha, \beta, \gamma, \delta$	matrix components of the unbounded domain linearized equations.
δ_h, δ_v	scale of nonconstant coefficient.
$\dot{\boldsymbol{\epsilon}}$	ice strain rate tensor.
$\dot{\boldsymbol{\epsilon}}_{II}$	second invariant of $\dot{\epsilon}$.
(κ_h, κ_e)	thickness and void ratio diffusion coefficients, equal to $(10^{-5}, 10^{-7})$.
μ	ice effective viscosity.
ν	basal heat conduction coefficient, equal to 0.001 W m^{-2}.
ρ	ice density, equal to 900 kg m^{-3}.
$\boldsymbol{\tau}$	ice deviatoric stress tensor.
$\boldsymbol{\tau}_b = (\tau^b_{xz}, \tau^b_{yz})$	bottom friction vector.
τ_0	till drag coefficient, equal to 10,327 Pa a m^{-1}.
ω	perturbation eigenvalue.
$F_{,xi}$	$\equiv \partial F / \partial x_i$.
$\overline{X}$	mean field of X.
X'	perturbation field of X.
X^*	dimensionless form of X.
$\Re, \Im$	real, imaginary operators.

[62] **Acknowledgments.** We thank Michael Ghil, Alan Rempel, Christian Schoof, Slawek Tulaczyk, Shreyas Mandre, and Rick O'Connell for very helpful discussions. We thank Christian Schoof, Richard Hindmarsh, and the Associate Editor for their knowledgeable and constructive reviews and Raphaella Serfaty for the illustration in Figure 1. This work was funded by the McDonnell Foundation and by the NSF paleoclimate program, grant ATM-0502482. E.T. thanks the Weizmann Institute where some of this work was done during a sabbatical.

References

Balmforth, N. J., R. V. Craster, and C. Toniolo (2003), Interfacial instability in non-Newtonian fluid layers, *Phys. Fluids*, *15*(11), 3370–3384.

Bamber, J., D. Vaughan, and I. Joughin (2000), Widespread complex flow in the interior of the Antarctic ice sheet, *Science*, *287*(5456), 1248–1250.

Baral, D. R., K. Hutter, and R. Greve (2001), Asymptotic theories of large-scale motion, temperature, and moisture distribution in land-based polythermal ice sheets: A critical review and new developments, *Appl. Mech. Rev.*, *54*(3), 215–256.

Bentley, C. R. (1987), Antarctic ice streams: A review, *J. Geophys. Res.*, *92*(B9), 8843–8858.

Bindschadler, R., J. Bamber, and S. Anandakrishnan (2001), Onset of streaming flow in the siple coast region, west Antarctica, in *The West Antarctic Ice Sheet: Behaviour and Environment*, *Antarct. Res. Ser.*, vol. 77, edited by R. B. Alley and R. A. Bindschadlerpp, pp. 123–136, AGU, Washington, D. C.

Clarke, G. K. C., U. Nitsan, and W. S. B. Paterson (1977), Strain heating and creep instability in glaciers and ice sheets, *Rev. Geophys.*, *15*(2), 235–247.

Dell'Isola, F., and K. Hutter (1998), What are the dominant thermomechanical processes in the basal sediment layer of large ice sheets?, *Proc. R. Soc. London, Ser. A*, *454*(1972), 1169–1195.

Echelmeyer, K., W. Harrison, C. Larsen, and J. Mitchell (1994), The role of the margins in the dynamics of an active ice stream, *J. Glaciol.*, *40*(136), 527–538.

Engelhardt, H., and B. Kamb (1997), Basal hydraulic system of a West Antarctic ice stream: Constraints from borehole observations, *J. Glaciol.*, *43*(144), 207–230.

Engelhardt, H., and B. Kamb (1998), Basal sliding of Ice Stream B, West Antarctica, *J. Glaciol.*, *44*(147), 223–230.

Engelhardt, H., N. Humphrey, B. Kamb, and M. Fahnestock (1990), Physical conditions at the base of a fast moving Antarctic ice stream, *Science*, *248*(4951), 57–59.

Fowler, A. C. (2003), On the rheology of till, *Ann. Glaciol.*, *37*, 55–59.

Fowler, A. C., and C. Johnson (1995), Hydraulic run-away—A mechanism for thermally regulated surges of ice sheets, *J. Glaciol.*, *41*(139), 554–561.

Fowler, A. C., and C. Johnson (1996), Ice sheet surging and ice stream formation, *Ann. Glaciol.*, *23*, 68–73.

Fowler, A. C., and D. A. Larson (1980), Thermal-stability properties of a model of glacier flow, *Geophys. J. R. Astron. Soc.*, *63*(2), 347–359.

Gagliardini, O., D. Cohen, P. Raback, and T. Zwinger (2007), Finite element modeling of subglacial cavities and related friction law, *J. Geophys. Res.*, *112*, F02027, doi:10.1029/2006JF000576.

Glen, J. W. (1952), Experiments on the deformation of ice, *J. Glaciol.*, *2*(12), 111–114.

Gudmundsson, G. H. (2003), Transmission of basal variability to a glacier surface, *J. Geophys. Res.*, *108*(B5), 2253, doi:10.1029/2002JB002107.

Haberman, R. (2004), *Applied Partial Differential Equations*, 4th ed., Prentice-Hall, Englewood Cliffs, N. J.

Hart, J., R. Hindmarsh, and G. Boulton (1990), Styles of subglacial glaciotectonic deformation within the context of the Anglian ice-sheet, *Earth Surf. Processes Landforms*, *15*(3), 227–241.

Hindmarsh, R. (1997), Deforming beds: Viscous and plastic scales of deformation, *Quat. Sci. Rev.*, *16*(9), 1039–1056.

Hindmarsh, R. (1998), Ice-stream surface texture, sticky spots, waves and breathers: The coupled flow of ice, till and water, *J. Glaciol.*, *44*(148), 589–614.

Hindmarsh, R. C. A. (2004a), Thermoviscous stability of ice-sheet flows, *J. Fluid Mech.*, *502*, 17–40.

Hindmarsh, R. C. A. (2004b), A numerical comparison of approximations to the Stokes equations used in ice sheet and glacier modeling, *J. Geophys. Res.*, *109*, F01012, doi:10.1029/2003JF000065.

Hindmarsh, R. C. A. (2006a), The role of membrane-like stresses in determining the stability and sensitivity of the Antarctic ice sheets: Back pressure and grounding line motion, *Philos. Trans. R. Soc. London, Ser. A*, *364*(1844), 1733–1767.

Hindmarsh, R. C. A. (2006b), Stress gradient damping of thermoviscous ice flow instabilities, *J. Geophys. Res.*, *111*, B12409, doi:10.1029/2005JB004019.

Hubbard, A., H. Blatter, P. Nienow, D. Mair, and B. Hubbard (1998), Comparison of a three-dimensional model for glacier flow with field data from Haut Glacier d'Arolla, Switzerland, *J. Glaciol.*, *44*(147), 368–378.

Hulton, N. R. J., and M. J. Mineter (2000), Modelling self-organization in ice streams, *Ann. Glaciol.*, *30*, 127–136.

Hutter, K. (1983), *Theoretical Glaciology*, D. Reidel, Hingham, Mass.

Huybrechts, P., T. Payne, and T. E. I. Group (1996), The EISMINT benchmarks for testing ice-sheet models, *Ann. Glaciol.*, *23*, 1–14.

Jackson, M., and B. Kamb (1997), The marginal shear stress of Ice Stream B, West Antarctica, *J. Glaciol.*, *43*(145), 415–426.

Jacobel, R. W., T. A. Scambos, C. F. Raymond, and A. M. Gades (1996), Changes in the configuration of ice stream flow from the West Antarctic Ice sheet, *J. Geophys. Res.*, *101*(B3), 5499–5504.

Jóhannesson, T. (1992), Landscape of temperate ice caps, Ph.D. thesis, Univ. of Wash., Seattle.

Kamb, B. (1991), Rheological nonlinearity and flow instability in the deforming bed mechanism of ice stream motion, *J. Geophys. Res.*, *96*(B10), 16,585–16,595.

Kamb, S. (2001), Basal zone of the West Antarctic ice streams and its role in lubrication of their rapid motion, in *The West Antarctic Ice Sheet: Behaviour and Environment*, *Antarct. Res. Ser.*, vol. 77, edited by R. B. Alley and R. A. Bindschadlerpp, pp. l57–l99, AGU, Washington, D. C.

Macayeal, D. R. (1989), Large-scale ice flow over a viscous basal sediment: Theory and application to Ice Stream-B, Antarctica, *J. Geophys. Res.*, *94*(B4), 4071–4087.

Macayeal, D. R. (1992), Irregular oscillations of the West Antarctic ice-sheet, *Nature*, *359*(6390), 29–32.

Marshall, S. J. (2005), Recent advances in understanding ice sheet dynamics, *Earth Planet. Sci. Lett.*, *240*(2), 191–204.

Marshall, S. J., and G. K. C. Clarke (1997), A continuum mixture model of ice stream thermomechanics in the Laurentide Ice Sheet: 2. Application to the Hudson Strait Ice stream, *J. Geophys. Res.*, *102*(B9), 20,615–20,637.

Nye, J. F. (1959), The motion of ice sheets and glaciers, *J. Glaciol.*, *3*(26), 493–507.

Nye, J. F. (1960), The response of glaciers and ice-sheets to seasonal and climatic changes, *Proc. R. Soc. London, Ser. A*, *256*(1287), 559–584.

Nye, J. F., and G. D. Q. Robin (1971), Causes and mechanics of glacier surges—Discussion, *Can. J. Earth Sci.*, *8*(2), 306–307.

Paterson, W. (1994), *The Physics of Glaciers*, 3rd ed., 480 pp., Pergamon, New York.

Pattyn, F. (1996), Numerical modeling of a fast flowing outlet glacier: Experiments with different basal conditions, *Ann. Glaciol.*, *23*, 237–246.

Pattyn, F. (2003), A new three-dimensional higher-order thermomechanical ice sheet model: Basic sensitivity, ice stream development, and ice flow across subglacial lakes, *J. Geophys. Res.*, *108*(B8), 2382, doi:10.1029/2002JB002329.

Payne, A. J., and P. W. Dongelmans (1997), Self-organization in the thermomechanical flow of ice sheets, *J. Geophys. Res.*, *102*(B6), 12,219–12,233.

Raymond, C., K. Echelmeyer, I. Whillans, and C. Doake (2001), Ice stream shear margins, in *The West Antarctic Ice Sheet: Behaviour and Environment*, *Antarct. Res. Ser.*, vol. 77, edited by R. B. Alley and R. A. Bindschadlerpp, pp. 137–155, AGU, Washington, D. C.

Ritz, C., V. Rommelaere, and C. Dumas (2001), Modeling the evolution of Antarctic ice sheet over the last 420,000 years: Implications for altitude changes in the Vostok region, *J. Geophys. Res.*, *106*(D23), 31,943–31,964.

Saito, F., A. Abe-Ouchi, and H. Blatter (2006), European Ice Sheet Modelling Initiative (EISMINT) model intercomparison experiments with first-order mechanics, *J. Geophys. Res.*, *111*, F02012, doi:10.1029/2004JF000273.

Schoof, C. (2004), On the mechanics of ice-stream shear margins, *J. Glaciol.*, *50*(169), 208–218.

Schoof, C. (2005), The effect of cavitation on glacier sliding, *Proc. R. Soc. London, Ser. A*, *461*(2055), 609–627.

Schoof, C. (2006), A variational approach to ice stream flow, *J. Fluid Mech.*, *556*, 227–251.

Tulaczyk, S., W. B. Kamb, and H. F. Engelhardt (2000a), Basal mechanics of Ice Stream B, West Antarctica: 1. Till mechanics, *J. Geophys. Res.*, *105*(B1), 463–481.

Tulaczyk, S., W. B. Kamb, and H. F. Engelhardt (2000b), Basal mechanics of Ice Stream B, West Antarctica: 2. Undrained plastic bed model, *J. Geophys. Res.*, *105*(B1), 483–494.

Whillans, I., C. Bentley, and C. van der Veen (2001), Ice Streams B and C, in *The West Antarctic Ice Sheet: Behaviour and Environment*, *Antarct. Res. Ser.*, vol. 77, edited by R. B. Alley and R. A. Bindschadlerpp, pp. 257–282, AGU, Washington, D. C.

Yuen, D., and G. Schubert (1979), The role of shear heating in the dynamics of large ice masses, *J. Glaciol.*, *24*, 195–212.

R. Sayag and E. Tziperman, Department of Earth and Planetary Science, Harvard University, Cambridge, MA 02138, USA. (sayag@fas.harvard.edu; eli@eps.harvard.edu)